

Phonon Coupled Scattering Caused Ultralow Lattice Thermal Conductivity and Its Role in The Remarkable Thermoelectric Performance of Newly Predicted SiS₂ and SiSe₂ monolayers

Jayanta Bera, Atanu Betal, Satyajit Sahu*

Department of Physics, Indian Institute of Technology Jodhpur, Jodhpur 342037, India

Abstract:

For high efficiency thermoelectric power conversion not only improvement of materials properties but also prediction and synthesis of new thermoelectric materials is needed. Here we have carried out a systematic investigation on thermoelectric performance of newly predicted two dimensional (2D) semiconducting SiS₂ and SiSe₂ monolayers of group IVA-VIA family using density functional theory (DFT) and Boltzmann transport equation (BTE). Our computed values of lattice thermal conductivity (k_{ph}) are ultralow which result very high thermoelectric figure of merit (ZT) value of 0.78 (0.80) at 500K in SiS₂ (SiSe₂) monolayer. The ultralow values of k_{ph} are attributed to phonon-phonon coupling of acoustic and low frequency optical branches which leads to larger scattering, low group velocity, smaller mean free path and shorter lifetime of phonons. It is also found from our investigation that p-type doping is more effective than n-type doping to get optimal power factor (PF) and ZT. Our theoretical investigation suggests that newly predicted semiconducting SiS₂ and SiSe₂ monolayers can be very promising thermoelectric materials for fabrication of high efficiency thermoelectric power generator to convert wastage heat into electricity.

1. Introduction:

Generation of thermoelectric power is a new environment-friendly technique of converting wastage heat into electricity. But its lower efficiency of conversion of heat into electricity makes it lagged behind the conventional source of electric power such as thermal power, wind power, solar power etc¹. So, search of materials with high thermoelectric PF and ZT to make optimal efficient thermoelectric power generator is a trending research now a days. The field of thermoelectric materials was mainly dominated by Skutterudites²⁻⁶ Clathrates⁷⁻¹⁰, complex alloys¹¹⁻¹³, metal chalcogenides and their alloys¹⁴⁻¹⁹ and some oxides²⁰⁻²² in last few decades. Among these Bi₂Te₃/Sb₂Te₃ superlattice²³, PbTe²⁴, SnSe²⁵ and Cu₂Se²⁶ are well known thermoelectric materials for their high ZT value. After the discovery of 2D graphene people are interested in other two-dimensional layered materials such as transition metal dichalcogenides (TMDCs), group IVA-VIA and group IVA-dihalides compounds MXenes and black phosphorus owing to unique electronic, optical, mechanical and thermoelectric properties^{27,28}. Two dimensional materials showed great potential in thermoelectric performance attributed to unique density of states (DOS) and fantastic combination of electrical conductivity (σ/τ) and k_{ph} ²⁹. Theoretical and experimental investigation on well-known TMDCs MoS₂³⁰ and WS₂³¹ monolayer suggest that in spite of high PF, the ZT is limited because of relatively high value of k_{ph} as compared to other TMDCS such as PtX₂³², HfX₂^{33,34}, SnX₂³⁵⁻³⁷ and ZrX₂³⁸ (where x = S and Se), whereas ultralow values of k_{ph} in PtX₂, HfX₂, SnX₂ and ZrX₂ result very high ZT greater than unity. Various efforts such as strain engineering³⁹⁻⁴¹ and chemical doping⁴² have been attempted for the enhancement of thermoelectric efficiency. Although these two-dimensional layered materials showed good thermoelectric behavior but there are still some shortcomings to achieve high efficiency in thermoelectric power generation. So, the improvement in material properties as well as prediction and synthesis of new type of materials are needed to increase the thermoelectric power efficiency. Beyond the graphene and 2D TMDCs, group IVA-VIA family of 2D materials such as SiS₂, SiSe₂, CS₂ and GeO₂, made with light elements become very popular recently⁴³. By using Ab initio calculation in association with molecular dynamics (MD) simulation electronic and structural properties of SiS₂ under pressure up to 100 GPa have been explored by Plašienka et al.⁴⁴. Recent experimental synthesis⁴⁵ of layered SiS₂ with octahedral coordination at 7.5-9.0 GPa by laser heating of elemental Si and S at 1300K to 1700K revealed that these type of group IVA-VIA layered compounds can be synthesized. A very recent theoretical prediction⁴³ of SiS₂

and SiSe₂ monolayer and their electronic properties with applied strain has been studied which motivates us to investigate the thermoelectric performance of these two materials.

In this work, we have performed a systematic study of structural, electronic properties and for the first time ever known we have investigated thermoelectric performance and lattice thermal conductivity (k_{ph}) in SiS₂ and SiSe₂ monolayer with the help of DFT and BTE. Our calculated values of k_{ph} in SiS₂ and SiSe₂ are 5.43 W/(mK) and 1.675 W/(mK) at 300K respectively which result a large ZT value of 0.66 (0.73) at 300K and 0.78 (0.80) at 500K in SiS₂ (SiSe₂) monolayer. It has also been observed that p-type doping is favorable for optimal thermoelectric performance in these two materials. The ultralow values of k_{ph} are attributed to phonon-phonon coupling which leads to larger scattering, low group velocity, smaller mean free path and shorter lifetime of phonons. Our theoretical calculation of high ZT and ultralow k_{ph} values suggests that newly predicted SiS₂ and SiSe₂ monolayers can have great potential to fabricate high efficiency thermoelectric power generator to convert wastage heat into electricity.

2. Computational Details:

First principle calculations were carried out using DFT⁴⁶ in Quantum Espresso (QE)⁴⁷ package. Ultrasoft pseudopotential for the electron-ion interactions and Perdew-Burke-Ernzerhof (PBE)⁴⁸ generalized gradient approximation (GGA)⁴⁹ as electronic exchange and correlation functional have been used throughout the calculations. A 18×18×1 dense k point sampling in hexagonal Brillouin zone (BZ) were used for the geometry relaxation of the unit cell whereas the cutoff energy for the plane wave function was kept at 50 Ry. For non-self-consistent (nscf) calculations a 60×60×1 dense k point sampling in BZ were used. Geometry relaxations were performed until the maximum force in individual atom reduced to a value of 0.01eV/Å. The effect of monolayer was implemented by creating sufficient vacuum of length 17 Å along the c direction to avoid interlayer interactions.

The thermoelectric properties have been calculated using BTE as implemented in BoltzTrap⁵⁰ code considering constant scattering time approximation (CSTA), which enables temperature and doping dependent electronic and thermal transport properties calculations assuming scattering time is unchanged with the energy. The details of the thermoelectric properties calculation can be found in our previous work³⁹. The linearized phonon Boltzmann equation was used to calculate the k_{ph}

in Phono3py⁵¹ interfaced to QE package⁴⁷. To calculate 3rd order anharmonic and 2nd order harmonic interatomic force constant $2 \times 2 \times 1$ supercell was used with $9 \times 9 \times 1$ k point sampling and for calculating k_{ph} $96 \times 96 \times 1$ k point sampling was used.

3. Results and discussions:

3.1. Structural parameters:

The unit cell of SiS_2 and SiSe_2 monolayers have a 1T- CdI_2 type crystal structures belonging to space group $P\bar{3}m1(164)$ where S or Se atoms are buckled in two different planes whereas Si atoms are sandwiched between two S or Se planes as shown in fig. 1a and fig. 1b. The optimized lattice constants of 3.30 Å (SiS_2) and 3.51 Å (SiSe_2) have been obtained from DFT with GGA-PBE functional. The Si-S bond length and S-Si-S bond angle have been calculated to be 2.312 Å and 89.5° in SiS_2 whereas Si-Se bond length and Se-Si-Se bond angle have been found to be 2.485 Å and 90.15° in SiSe_2 monolayer. Our calculated values of lattice constant, bond lengths and bond angles match very well with previous computed data⁴³.

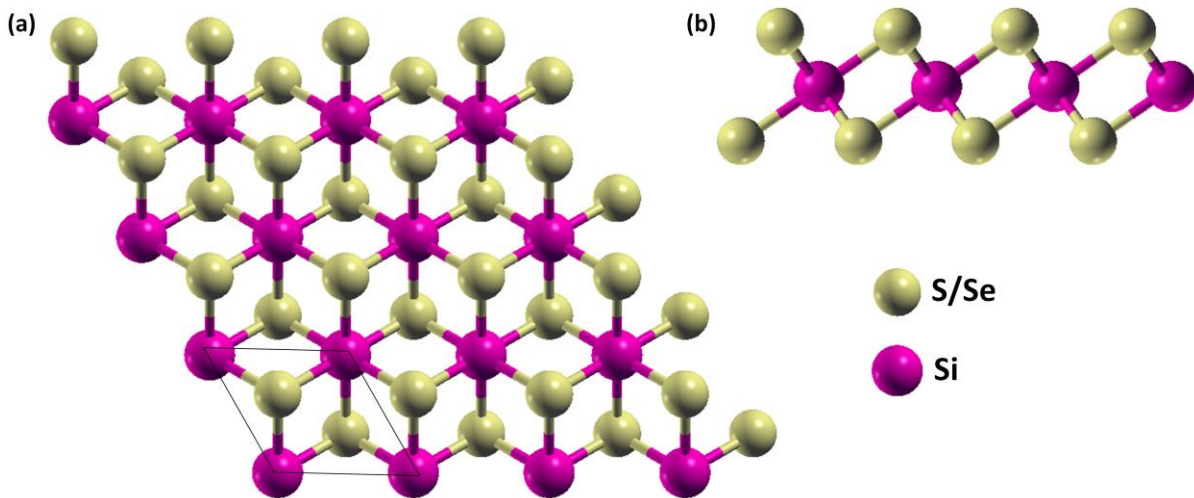


Fig. 1. (a) Top view and (b) side view of a $4 \times 4 \times 1$ supercell SiX_2 ($X=\text{S/Se}$) monolayer. The hexagonal unit cell is shown by black box.

3.2. Structural stability:

3.2.1. Cohesive energy:

To find the structural stability of our structures we have calculated the cohesive energy per atom (E_C) using the expression

$$E_C = [E_{\text{Si}} + 2E_{\text{S/Se}} - E_{\text{SiS}_2/\text{SiSe}_2}]/3, \quad (1)$$

where E_{Si} and $E_{\text{S/Se}}$ are the total ground state energy of a single Si atom and a single S or Se atom and $E_{\text{SiS}_2/\text{SiSe}_2}$ is the total ground state energy of the SiS_2 or SiSe_2 unit cell. From our calculations cohesive energy per atom of SiS_2 and SiSe_2 has been found with a value of 5.08 eV/atom and 4.46 eV/atom respectively which is in good agreement with previous calculation⁴³. Our calculated values are comparable with other 2D materials such as graphene (8.00 eV/atom)⁵², silicene (3.94 eV/atom)⁵³, phosphorene (3.44 eV/atom)⁵⁴, WS_2 (2.87 eV/atom)³⁹ and Be_2C monolayer (4.84 eV/atom)⁵⁵ which suggest very good structural stabilities of the considered structures.

3.2.2. Phonon dispersion curve:

Phonon dispersion curves of SiS_2 and SiSe_2 have been plotted along the hexagonal BZ path Γ -M-K- Γ as shown in Fig. 2a and Fig. 2b respectively. There is a very small frequency domain in the negative side (-2 cm^{-1} in SiS_2 and -3 cm^{-1} in SiSe_2 at Γ point) which suggests that the structures are dynamically stable. The highest frequencies of 17.24 THz (575 cm^{-1}) and 14 THz (467 cm^{-1}) have been calculated for SiS_2 and SiSe_2 respectively and it is clear that SiSe_2 has lower frequency than that of SiS_2 . It is also seen that the acoustic branches are coupled to the nearest optical branches in both materials. The acoustic branches are contributed mainly by the S or Se atoms whereas optical branches are contributed by combination of Si and S or Se atoms as seen from the projected PhDOS plot. Since, Se atoms are heavier than S atoms and will vibrate with lower frequency than that of S atoms hence SiSe_2 monolayer has lower phonon frequency than that of SiS_2 monolayer.

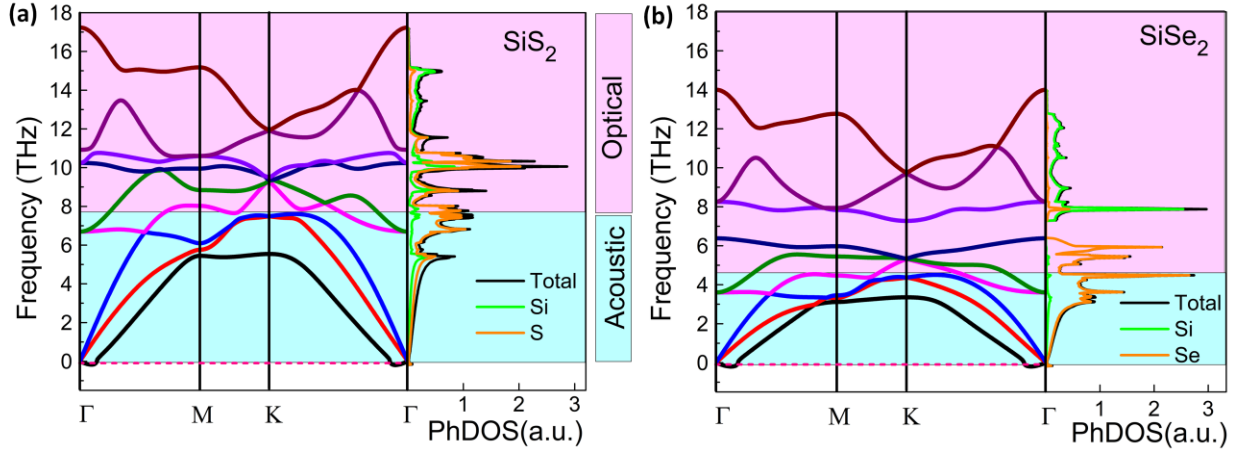


Fig. 2. Phonon dispersion curves and PhDOS of (a) SiS_2 and (b) SiSe_2 . The black, red and blue line in the dispersion curves act for out of plane acoustic (ZA), transverse acoustic (TA) and longitudinal acoustic (LA) modes respectively.

3.3. Electronic band structures:

The electronic band structures of monolayer SiS_2 and SiSe_2 have been calculated using GGA-PBE along high symmetry path Γ -M-K- Γ in hexagonal BZ as shown in Fig. 3a and Fig. 3b. Both the structures show semiconducting indirect band gap as conduction band minima (CBM) lies on M point whereas valance band maxima (VBM) lies in between high symmetry points Γ and M. An indirect band gap of 1.39 eV and 0.48 eV have been calculated in SiS_2 and SiSe_2 monolayer respectively which are very close to the values with previous PBE calculations but lower as compared to the band gap calculated⁴³ (2.45 eV for SiS_2 and 1.37 eV for SiSe_2) with HSE06 functional. This is because PBE underestimates the band gap. To find the contribution of Si and S or Se atom on the electronic properties of SiS_2 and SiSe_2 monolayers, projected DOS (PDOS) has been calculated as shown in Fig. 3c and Fig. 3d. As seen from total DOS of both the structures it is clear that density of states is higher in valance band as compared to conduction band. The gap between valance band states and conduction band states are much higher in SiS_2 as compared to SiSe_2 as band gap is higher in SiS_2 . It is also clear that both valance and conduction band are mostly dominated by 2p and 3p orbitals of chalcogenide S and Se atoms respectively whereas very small contribution of Si atoms near the band edges has been observed in SiS_2 and SiSe_2 monolayers. We have also plotted two-dimensional charge density as shown in Fig. 4 where one can clearly see that charges are localized mostly on S or Se atoms and less amount of charge on Si

atoms. Therefore, S (Se) plays significant role than that of Si atoms in electronic properties of SiS₂ (SiSe₂) monolayers. It is also noted, that strong polar covalent type of Si-S(Se) bonding in these monolayers is owing to the electronegativity difference of Si, S and Se atoms.

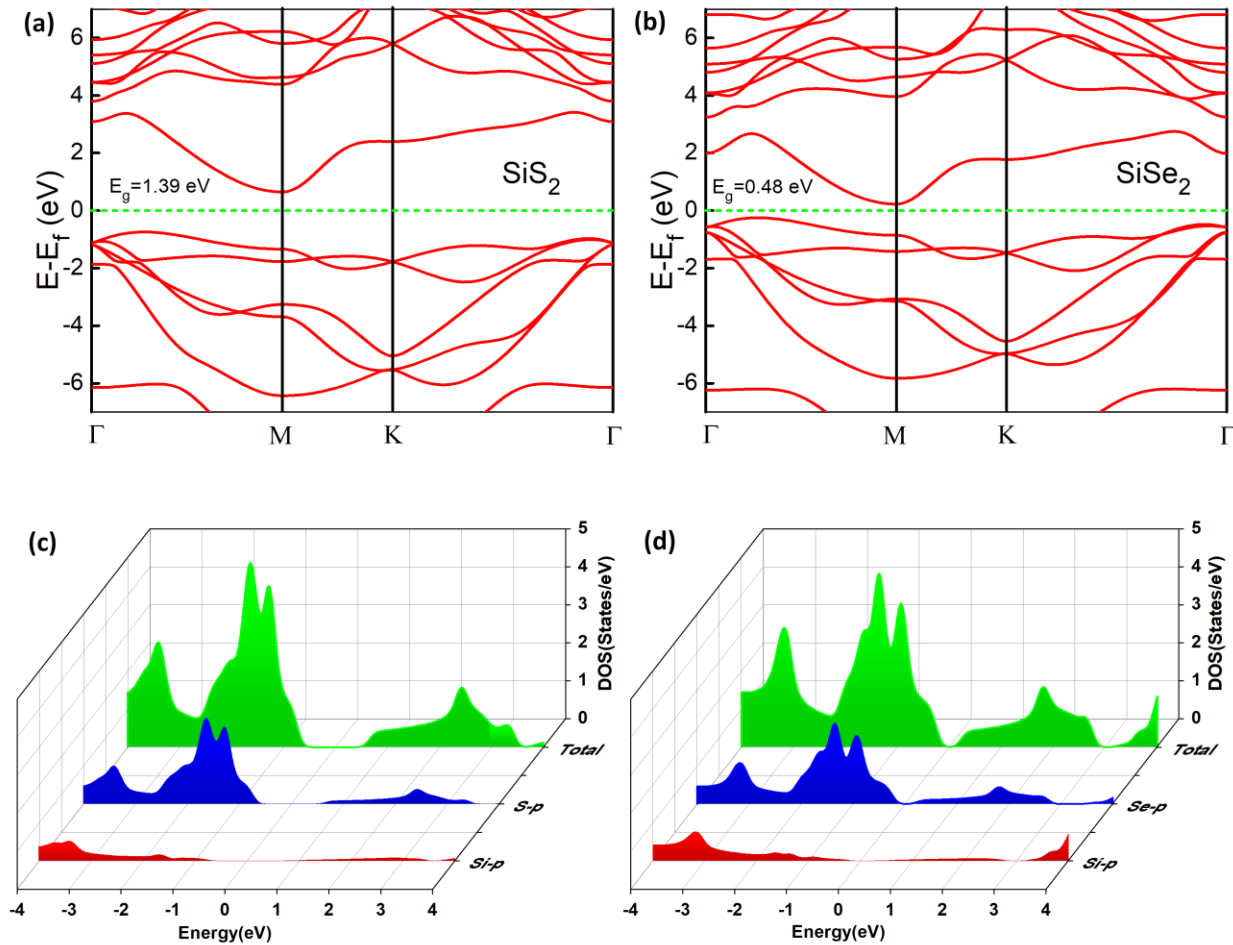


Fig. 3. Electronic band structures of (a) SiS₂ (b) SiSe₂ monolayers with PBE. PDOS of (c) SiS₂ (d) SiSe₂ monolayers.

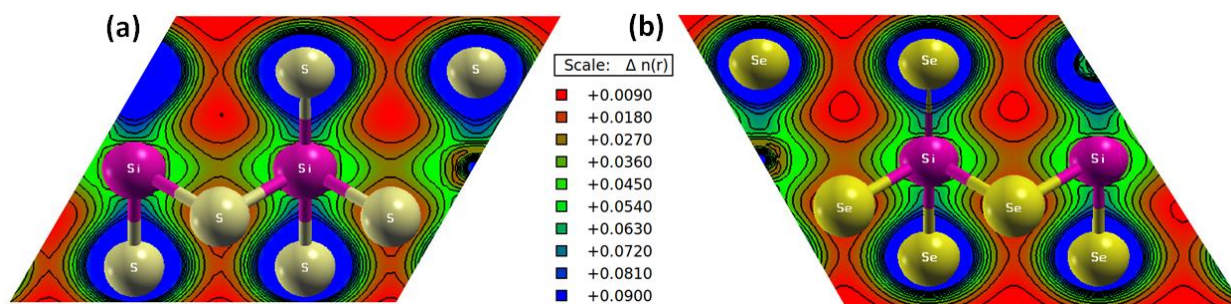


Fig. 4. Two-dimensional charge density plot of (a) SiS₂ and (b) SiSe₂ monolayers.

3.4. Carrier's mobility and relaxation time:

To calculate the mobility of carriers in the structures, deformation potential (E_l) theory as proposed by Bardeen and Shockley⁵⁶ has been used. As stated in this theory, mobility of two-dimensional materials (μ_{2D}) can be determined as

$$\mu_{2D} = \frac{e\hbar^3 C_{2D}}{K_B T m^* m_d^* (E_l^2)} \quad (2)$$

where \hbar , K_B , e and T are the Planck's constant, Boltzmann constant, elementary charge and temperature respectively. The elastic constant C_{2D} is defined as $C_{2D} = [\partial^2 E / \partial \varepsilon^2] / A_0$ where E , ε and A_0 are total energy, amount of uni-axial strain and the optimized cell's area respectively. $m^* = \hbar^2 / [\partial^2 E / \partial k^2]$ is the effective mass along the propagation direction and $m_d^* = \sqrt{m_{\parallel} m_{\perp}}$ where m_{\parallel} (m_{\perp}) is the effective mass parallel (perpendicular) to the propagation direction. E_l can be obtained for electron and hole by calculating the amount of shift in CBM and VBM in terms of energy with applied strain as shown in Fig. 5c and 5d. The relaxation time can be determined in terms of mobility as $\tau = m^* \mu / e$. The effective mass of the electron and hole are anisotropic in nature in SiS₂ and SiSe₂. Our theoretical calculation reveals that SiS₂ and SiSe₂ have high carrier mobility of the order of $\sim 10^3 \text{ cm}^2 \text{V}^{-1} \text{s}^{-1}$. Our calculated values of mobility are higher than mobility of popular two-dimensional TMDC MoS₂ ($200 \text{ cm}^2 \text{V}^{-1} \text{s}^{-1}$)⁵⁷ and comparable to other 2D materials such as phosphorene ($1.0 \times 10^3 \text{ cm}^2 \text{V}^{-1} \text{s}^{-1}$)⁵⁸, GeS monolayer ($3.7 \times 10^3 \text{ cm}^2 \text{V}^{-1} \text{s}^{-1}$)⁵⁹ and GeTe monolayer ($1.0 \times 10^3 \text{ cm}^2 \text{V}^{-1} \text{s}^{-1}$)⁶⁰. All the parameters related to mobility are listed in Table 2.

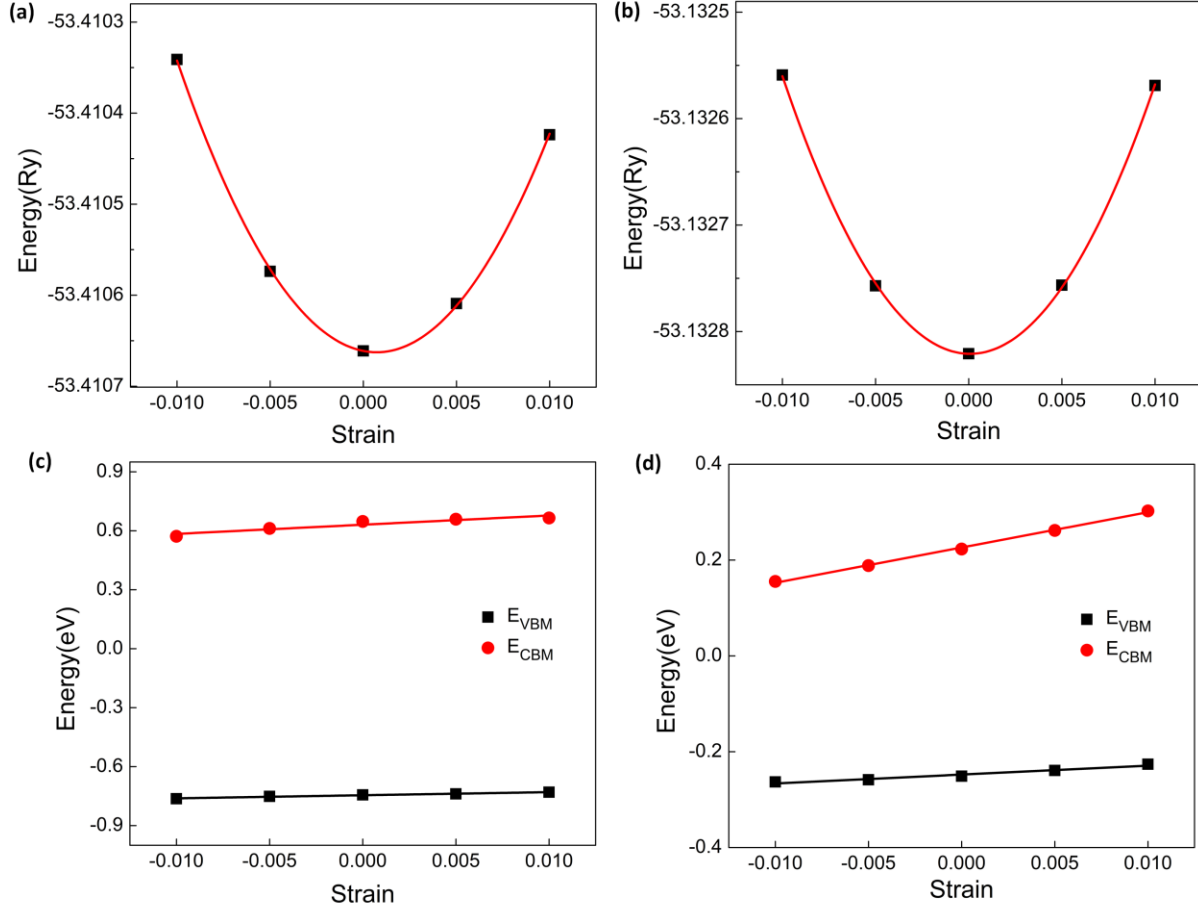


Fig. 5. Variation of total energy with uni-axial strain in (a) SiS₂ and (b) SiSe₂. Shift in the CBM and VBM in eV with uni-axial strain in (c) SiS₂ and (d) SiSe₂ to determine deformation potential.

Sample	Carrier	$m_{\Gamma-M}^*$	m_{K-M}^*	C_{2D} (N/m)	E_l (eV)	μ_{2D} (cm ² V ⁻¹ s ⁻¹)	τ (s) × 10 ⁻¹³
SiS ₂	electron	0.43	0.14	129	4.678	3664	3.00
	hole	0.54	1.25	129	1.577	1079	7.68
SiSe ₂	electron	0.41	0.14	105	7.359	1233	0.98
	hole	0.52	0.93	105	1.864	997	5.30

Table 2. Calculated values of effective mass, C_{2D} , E_l , μ_{2D} and τ of electrons and holes in monolayer SiS₂, SiSe₂.

3.5. Thermoelectric performance:

To find the thermoelectric performance of monolayer SiS₂ and SiSe₂, the variation of Seebeck coefficient (S), relaxation time scaled electrical conductivity (σ/τ), electronic thermal conductivity (K_{el}/τ) and PF($S^2\sigma/\tau$) as a function of chemical potential (μ) at 300K to 500K have been plotted in Fig. 6a and Fig. 6b respectively. The highest S value of 2100 $\mu\text{V/K}$ (n-type) and 2281 $\mu\text{V/K}$ (p-type) in SiS₂ and 654 $\mu\text{V/K}$ (n-type) and 802 $\mu\text{V/K}$ (p-type) in SiSe₂ at 300K has been calculated. S is higher in SiS₂ than that of SiSe₂ because S depends on band gap and SiSe₂ has a lower band gap. As temperatures rises the value of S drops whereas σ/τ and K_{el}/τ increase with rising temperature. The thermoelectric power factor (PF) has been calculated to be 15.61 $\text{Wm}^{-1}\text{K}^{-2}\text{s}^{-1}$ (p-type) and 7.71 $\text{Wm}^{-1}\text{K}^{-2}\text{s}^{-1}$ (n-type) in SiS₂ and 15.55 $\text{Wm}^{-1}\text{K}^{-2}\text{s}^{-1}$ (p-type) and 7.77 $\text{Wm}^{-1}\text{K}^{-2}\text{s}^{-1}$ (n-type) in SiSe₂ monolayer at 300K. So, it is obvious that the PF for p-type carriers are almost double that of n-type carriers in both the materials at 300K suggesting p-type semiconducting nature of these monolayers. The reason of this type of behavior can be found from the total DOS as shown in Fig. 3c and Fig. 3d where it is clearly seen that the number of energy states per eV in the valance band are much higher than that in conduction band. At 500K, highest PF of 22.96 $\text{Wm}^{-1}\text{K}^{-2}\text{s}^{-1}$ and 23.04 $\text{Wm}^{-1}\text{K}^{-2}\text{s}^{-1}$ for p-type carriers in SiS₂ and SiSe₂ monolayers respectively has been obtained. So, for both materials S and PF for p-type is much higher than that of n-type which suggest p-type doping is more effective than n-type to get optimum thermoelectric performance in these monolayers. In contrast, n-type doping is preferable for thermoelectric application in popular two-dimensional TMDCs thermometric materials such as MoS₂⁶¹ and WS₂³⁹.

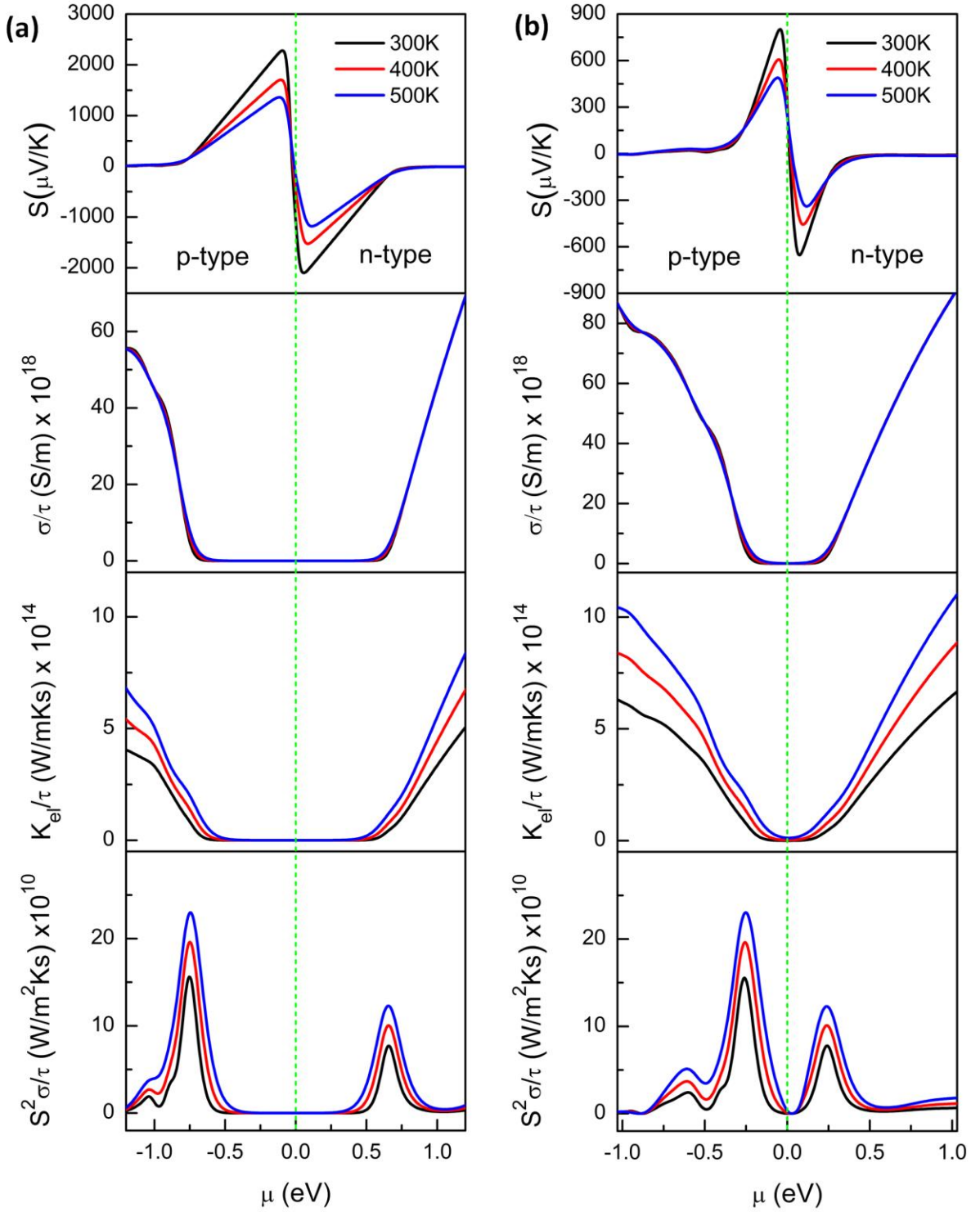


Fig. 6. Variation of S , σ/τ , K_{el}/τ and $S^2\sigma/\tau$ as a function of μ at 300K to 500K in (a) SiS_2 and (b) SiSe_2 monolayers. Fermi level is shown by green dashed lines.

3.6. Lattice thermal conductivity (k_{ph}):

The variation of k_{ph} with temperature in SiS₂ and SiSe₂ has been plotted in Fig. 7a and k_{ph} varies as T^{-1} with temperature owing to phonon-phonon scattering. Our calculated values of k_{ph} in SiS₂ and SiSe₂ are 5.43 W/(mK) and 1.675 W/(mK) at 300K respectively. Our calculated ultralow values of k_{ph} are comparable with well-known high-performance thermoelectric materials such as Bi₂Te₃ ($k_{ph}=1.6$ W/mK)⁶², PbTe ($k_{ph}=2.2$ W/mK)⁶³ and SnSe ($k_{ph}=2.6$ W/mK)⁶⁴ and much lower than popular 2D TMDCs MoS₂ ($k_{ph}=34.5$ W/mK)⁶⁵ and WS₂ ($k_{ph}=72$ W/mK)³⁹. To investigate the origin of ultralow values of k_{ph} we have to look into the phonon dispersion curves as shown previously in Fig. 2. It is clear from phonon dispersion curves of both the materials that unlike MoS₂ and WS₂, there is no gap between acoustic and optical branches and the acoustic branches are coupled to the optical branches in monolayer SiS₂ and SiSe₂. In MoS₂, WS₂, MoSe₂ and WSe₂^{66,67} there is a finite gap between acoustic and optical branches. Due to this coupling phonon-phonon scattering increases and group velocity (v_g) and mean free path (MFP) of phonons decrease which induce low values of k_{ph} in SiS₂ and SiSe₂ monolayer.

The cumulative k_{ph} and its derivative have been plotted as a function of phonon frequency and shown in Fig. 7b. It is clearly seen that k_{ph} becomes almost constant around 6 THz in SiSe₂ whereas it became constant around 10 THz in SiS₂. So, in both the monolayers acoustic modes which are in the lower frequency region (as shown by cyan colour in Fig. 2) have more effect on k_{ph} than that of optical modes. Also, phonons have lower frequency in SiSe₂ than in SiS₂ because of larger atomic mass of Se than S atoms. To find the contribution of phonons with different MFP we have plotted cumulative k_{ph} divided by total k_{ph} as a function of phonon MFP as shown in Fig. 7c. where the blue and red colours have been used for SiS₂ and SiSe₂ respectively. It has been observed that almost 90% of the total k_{ph} values are contributed by those phonons which have MFP less than 623Å in SiS₂ and 185Å in SiSe₂ monolayer. Therefore, it is clear that phonons have much smaller MFP and which will result stronger scattering and induce lower k_{ph} in SiSe₂ than that in SiS₂.

The mode dependent v_g as a function of phonon frequency has been plotted in Fig. 7d and Fig. 7e for SiS₂ and SiSe₂ monolayer respectively. The group velocity of both acoustic and optical phonon branches is lower in SiSe₂ than that of SiS₂ which means the phonons move with smaller group velocity in SiSe₂. The smaller group velocity of phonons also induces lower k_{ph} in SiSe₂ monolayers. Almost 90% of the k_{ph} is contributed by acoustic branches and 10% by optical branches in both the monolayers as shown in Fig. 8. ZA branches contribute more among the acoustic branches owing to the lower group velocity of ZA branch than TA and LA branch. Phonon lifetime as a function of frequency has been shown in Fig. 9. and it is observed that phonon lifetime of SiSe₂ is shorter than SiS₂. Therefore, lower group velocity, smaller MFP and shorter lifetime of phonons result stronger scattering of phonons which induce lower value of k_{ph} in SiSe₂ than that of SiS₂.

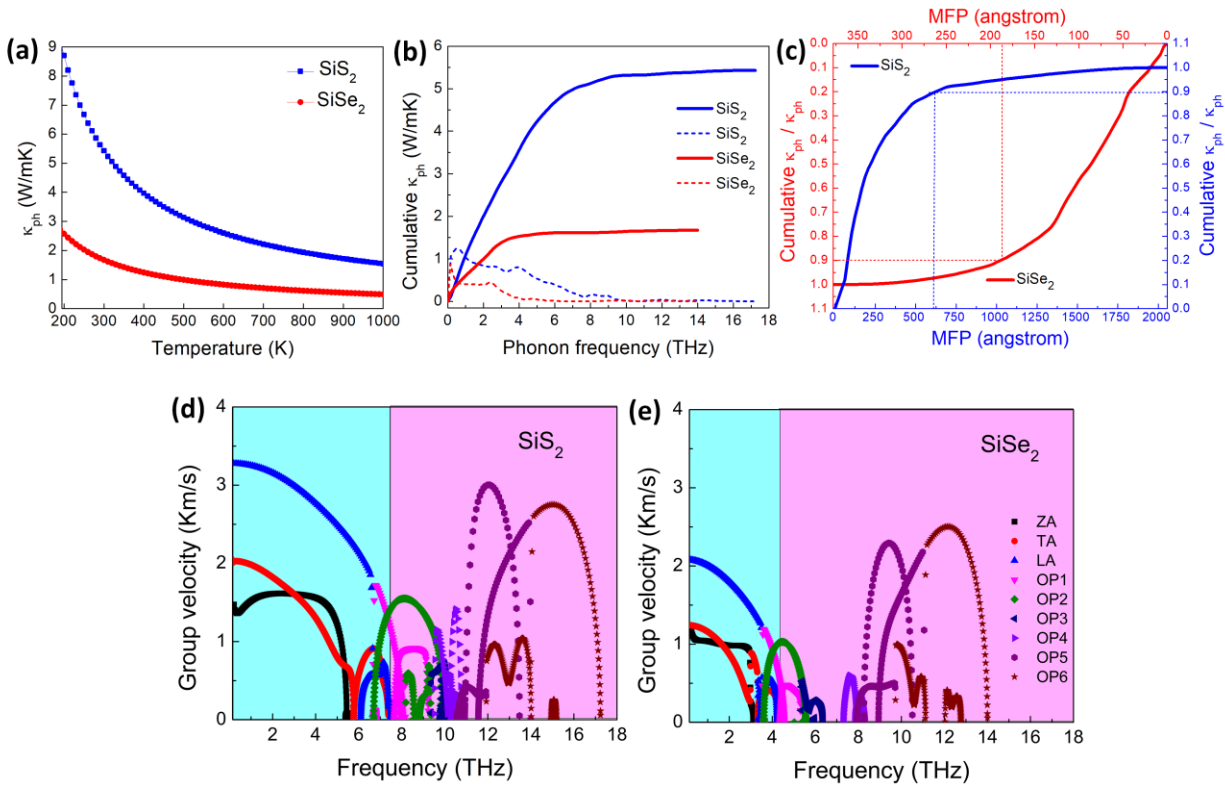


Fig.7. (a) Variation of k_{ph} with temperature (b) cumulative k_{ph} and its derivative (shown by dashed lines) as a function of phonon frequency and (c) cumulative k_{ph} divided by total k_{ph} as a function of MFP in SiS₂ and SiSe₂ monolayer. Group velocity of different phonon modes as a

function of frequency in (d) SiS₂ and (e) SiSe₂ where cyan and magenta colored regions represent acoustic and optical branches respectively.

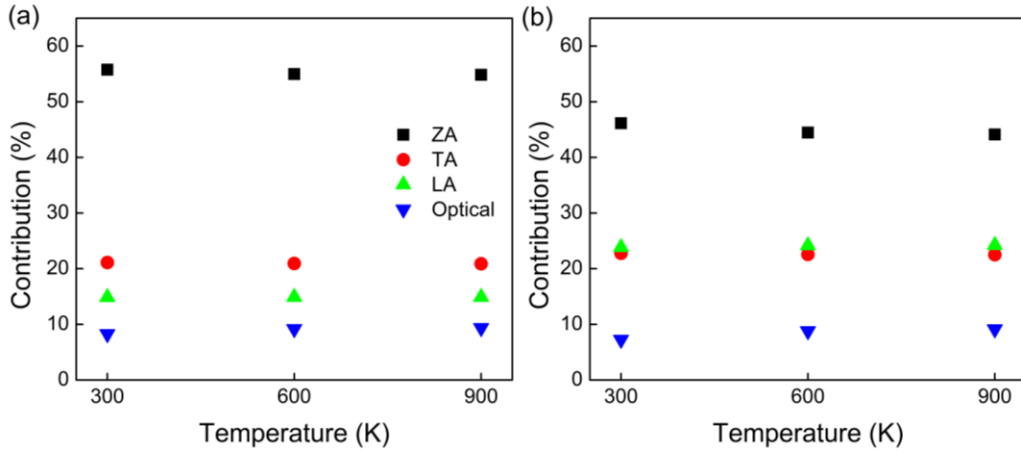


Fig.8. Percentage contribution of different phonon modes to the total k_{ph} in (a) SiS₂ and (b) SiSe₂.

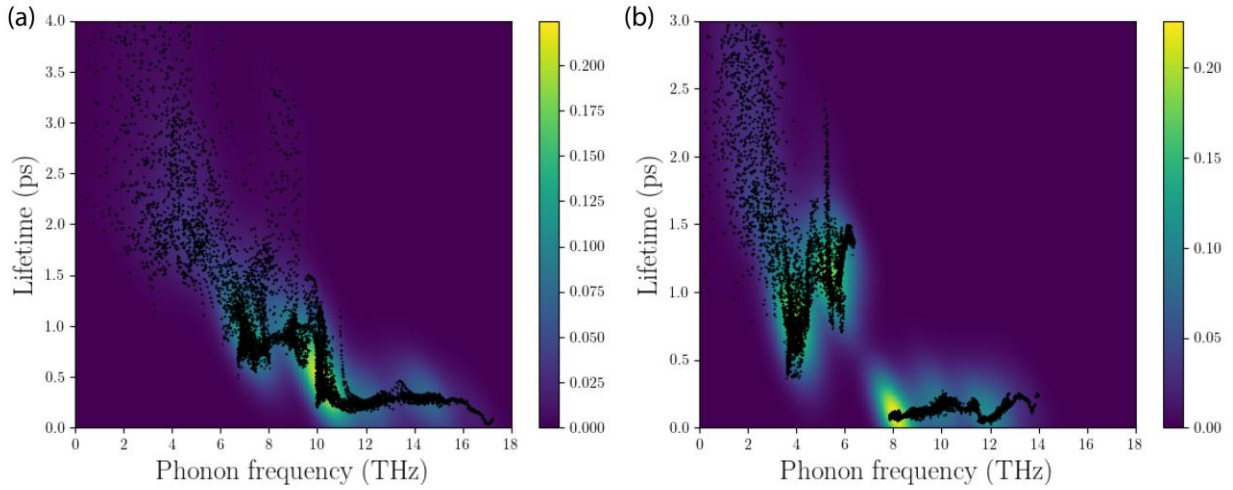


Fig. 9. Phonon lifetime in pico-second as a function of phonon frequency in Tera-Hertz in (a) SiS₂ and (b) SiSe₂ monolayers.

3.7. Thermoelectric figure of merit (ZT):

The term ZT defines the quality of a thermoelectric material and can be expressed by

$$ZT = \frac{S^2 \sigma T}{K_{el} + k_{ph}}$$

where all the parameters are defined in previous sections. The variation of ZT as a function of μ (eV) in SiS₂ and SiSe₂ are shown in Fig. 10a and Fig. 10b respectively. We have calculated ZT value of 0.66 in SiS₂ and 0.73 in SiSe₂ respectively at 300K for p-type carriers. These values are very high at 300K and we have calculated highest ZT value of 0.78 and 0.80 in SiS₂ and SiSe₂ respectively for p-type carriers at 500K. All the ZT values are listed in Table 3. Like PF values, ZT values are also higher for p-type carriers than n-type, which indicates that p-type doping is favorable for optimal thermoelectric performance in SiS₂ and SiSe₂ monolayers to achieve maximum ZT. SiSe₂ has slightly higher ZT value as compared to SiS₂, because of lower value of k_{ph} owing to lower group velocity, lower MFP and stronger scattering in SiSe₂ as discussed in previous section. So, these high values of ZT at room temperature (300K) and slightly higher temperature (500K) reveals that monolayer SiS₂ and SiSe₂ can be used as highly efficient thermoelectric materials operating near room temperature.

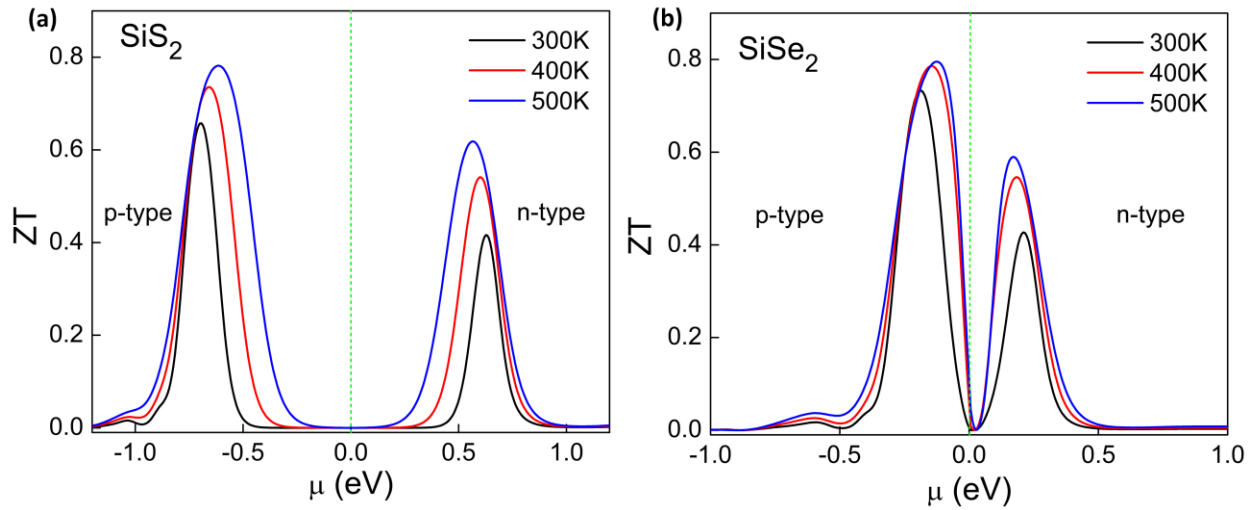


Fig. 10. Variation of ZT as a function of μ at 300K to 500K in (a) SiS₂ and (b) SiSe₂ monolayers.

Sample		S (μ V/K)			$S^2\sigma/\tau$ (W/mK ² s) $\times 10^{10}$			ZT		
		300K	400K	500K	300K	400K	500K	300K	400K	500K
SiS ₂	n	2100	1524	1180	7.71	10.03	12.29	0.42	0.54	0.62

	p	2281	1706	1361	15.61	19.60	22.96	0.66	0.73	0.78
SiSe₂	n	654	457	339	7.77	10.10	12.28	0.43	0.55	0.59
	p	802	606	488	15.55	19.61	23.04	0.73	0.78	0.80

Table 3. Calculated values of S , $S^2\sigma/\tau$ and ZT at 300K, 400K and 500K in monolayer SiS_2 and SiSe_2 .

4. Conclusions:

In summary, a systematic investigation of electronic, structural and thermoelectric properties of newly predicted monolayers SiS_2 and SiSe_2 has been carried out with the help of DFT and BTE. Our calculated ultralow values of k_{ph} at 300K in SiS_2 and SiSe_2 are 5.43 W/(mK) and 1.675 W/(mK) respectively. These ultralow values of k_{ph} are attributed to phonon-phonon coupling of acoustic and optical branches which leads to larger scattering, low group velocity, smaller mean free path and shorter lifetime of phonons. High PF for p-type carriers and ultralow k_{ph} result high ZT values of 0.78 (0.80) at 500K in SiS_2 (SiSe_2) monolayer. From our investigation it has been found that p-type doping is more effective than n-type doping in both the materials of our interest to get optimal ZT and PF. Our calculated carrier mobility values are high which are in the orders of $\sim 10^3 \text{ cm}^2\text{V}^{-1}\text{s}^{-1}$ for these two materials. From our investigation it is clear that newly predicted semiconducting monolayer SiS_2 and SiSe_2 could be very promising new generation thermoelectric materials for fabrication of high efficiency thermoelectric power generator to convert wastage heat into electricity.

Conflicts of interest

There are no conflicts to declare.

Acknowledgement:

The authors are thankful to Ministry of Human Resource and Development (MHRD) for supporting the work and IIT Jodhpur for providing the necessary infrastructure to carry out the research.

Author contributions

J.B. conceived the idea and performed the first principle calculations of the materials. J.B. also wrote the paper. A.B. helped in studying some properties of the materials. S.S. helped in writing the paper and editing the paper.

References:

- 1 L. Yang, Z. Chen, M. S. Dargusch and J. Zou, High performance thermoelectric materials: progress and their applications, *Adv. Energy Mater.*, 2018, **8**, 1701797.
- 2 B. C. Sales, D. Mandrus and R. K. Williams, Filled skutterudite antimonides: a new class of thermoelectric materials, *Science (80-.)*, 1996, **272**, 1325–1328.
- 3 X. Shi, J. Yang, J. R. Salvador, M. Chi, J. Y. Cho, H. Wang, S. Bai, J. Yang, W. Zhang and L. Chen, Multiple-filled skutterudites: high thermoelectric figure of merit through separately optimizing electrical and thermal transports, *J. Am. Chem. Soc.*, 2011, **133**, 7837–7846.
- 4 L. Bertini, C. Stiewe, M. Toprak, S. Williams, D. Platzek, A. Mrotzek, Y. Zhang, C. Gatti, E. Müller and M. Muhammed, Nanostructured $\text{Co}_{1-x}\text{Ni}_x\text{Sb}_3$ skutterudites: synthesis, thermoelectric properties, and theoretical modeling, *J. Appl. Phys.*, 2003, **93**, 438–447.
- 5 B. C. Sales, B. C. Chakoumakos and D. Mandrus, Thermoelectric properties of thallium-filled skutterudites, *Phys. Rev. B*, 2000, **61**, 2475.
- 6 X. Meng, Z. Liu, B. Cui, D. Qin, H. Geng, W. Cai, L. Fu, J. He, Z. Ren and J. Sui, Grain boundary engineering for achieving high thermoelectric performance in n-type skutterudites, *Adv. Energy Mater.*, 2017, **7**, 1602582.
- 7 Y. Liu, L. Wu, L. Li, S. Du, J. D. Corbett and L. Chen, The Antimony-Based Type I Clathrate Compounds $\text{Cs}_8\text{Cd}_{18}\text{Sb}_{28}$ and $\text{Cs}_8\text{Zn}_{18}\text{Sb}_{28}$, *Angew. Chemie*, 2009, **121**,

- 5409–5412.
- 8 H. Kleinke, New bulk materials for thermoelectric power generation: clathrates and complex antimonides, *Chem. Mater.*, 2010, **22**, 604–611.
 - 9 M. Christensen, S. Johnsen and B. B. Iversen, Thermoelectric clathrates of type I, *Dalt. Trans.*, 2010, **39**, 978–992.
 - 10 A. Saramat, G. Svensson, A. E. C. Palmqvist, C. Stiewe, E. Müller, D. Platzek, S. G. K. Williams, D. M. Rowe, J. D. Bryan and G. D. Stucky, Large thermoelectric figure of merit at high temperature in Czochralski-grown clathrate Ba₈Ga₁₆Ge₃₀, *J. Appl. Phys.*, 2006, **99**, 23708.
 - 11 G. J. Snyder, M. Christensen, E. Nishibori, T. Caillat and B. B. Iversen, Disordered zinc in Zn₄Sb₃ with phonon-glass and electron-crystal thermoelectric properties, *Nat. Mater.*, 2004, **3**, 458–463.
 - 12 C. Fu, S. Bai, Y. Liu, Y. Tang, L. Chen, X. Zhao and T. Zhu, Realizing high figure of merit in heavy-band p-type half-Heusler thermoelectric materials, *Nat. Commun.*, 2015, **6**, 1–7.
 - 13 A. Tengå, S. Lidin, J.-P. Belieres, N. Newman, Y. Wu and U. Häussermann, Metastable Cd₄Sb₃: A complex structured intermetallic compound with semiconductor properties, *J. Am. Chem. Soc.*, 2008, **130**, 15564–15572.
 - 14 L. Hu, H. Wu, T. Zhu, C. Fu, J. He, P. Ying and X. Zhao, Tuning multiscale microstructures to enhance thermoelectric performance of n-type Bismuth-Telluride-based solid solutions, *Adv. Energy Mater.*, 2015, **5**, 1500411.
 - 15 H. Liu, X. Shi, F. Xu, L. Zhang, W. Zhang, L. Chen, Q. Li, C. Uher, T. Day and G. J. Snyder, Copper ion liquid-like thermoelectrics, *Nat. Mater.*, 2012, **11**, 422–425.
 - 16 J.-S. Rhyee, K. H. Lee, S. M. Lee, E. Cho, S. Il Kim, E. Lee, Y. S. Kwon, J. H. Shim and G. Kotliar, Peierls distortion as a route to high thermoelectric performance in In₄Se_{3-δ} crystals, *Nature*, 2009, **459**, 965–968.

- 17 B. Poudel, Q. Hao, Y. Ma, Y. Lan, A. Minnich, B. Yu, X. Yan, D. Wang, A. Muto and D. Vashaee, High-thermoelectric performance of nanostructured bismuth antimony telluride bulk alloys, *Science* (80-.), 2008, **320**, 634–638.
- 18 S. H. Yang, T. J. Zhu, T. Sun, J. He, S. N. Zhang and X. B. Zhao, Nanostructures in high-performance (GeTe) x (AgSbTe₂) 100– x thermoelectric materials, *Nanotechnology*, 2008, **19**, 245707.
- 19 L.-D. Zhao, S.-H. Lo, Y. Zhang, H. Sun, G. Tan, C. Uher, C. Wolverton, V. P. Dravid and M. G. Kanatzidis, Ultralow thermal conductivity and high thermoelectric figure of merit in SnSe crystals, *Nature*, 2014, **508**, 373–377.
- 20 S. Maensiri and W. Nuansing, Thermoelectric oxide NaCo₂O₄ nanofibers fabricated by electrospinning, *Mater. Chem. Phys.*, 2006, **99**, 104–108.
- 21 R. Robert, S. Romer, A. Reller and A. Weidenkaff, Nanostructured complex cobalt oxides as potential materials for solar thermoelectric power generators, *Adv. Eng. Mater.*, 2005, **7**, 303–308.
- 22 Y. Wang, N. S. Rogado, R. J. Cava and N. P. Ong, Spin entropy as the likely source of enhanced thermopower in Na x Co 2 O 4, *Nature*, 2003, **423**, 425–428.
- 23 R. Venkatasubramanian, E. Siivola, T. Colpitts and B. O’ Quinn, Thin-Film Thermoelectric Devices with High Room-Temperature Figures of Merit, *Nature*, 2001, **413**, 597–602.
- 24 K. Biswas, J. He, I. D. Blum, C.-I. Wu, T. P. Hogan, D. N. Seidman, V. P. Dravid and M. G. Kanatzidis, High-performance bulk thermoelectrics with all-scale hierarchical architectures, *Nature*, 2012, **489**, 414–418.
- 25 A. T. Duong, G. Duvjir, S. Kwon, J. Y. Song, J. K. Lee, J. E. Lee, S. Park, T. Min, J. Lee and J. Kim, Achieving ZT= 2.2 with Bi-doped n-type SnSe single crystals, *Nat. Commun.*, 2016, **7**, 1–6.
- 26 H. Liu, X. Yuan, P. Lu, X. Shi, F. Xu, Y. He, Y. Tang, S. Bai, W. Zhang and L. Chen, Ultrahigh thermoelectric performance by electron and phonon critical scattering in

- Cu₂Se_{1-x}I_x, *Adv. Mater.*, 2013, **25**, 6607–6612.
- 27 S. Z. Butler, S. M. Hollen, L. Cao, Y. Cui, J. A. Gupta, H. R. Gutiérrez, T. F. Heinz, S. S. Hong, J. Huang and A. F. Ismach, Progress, challenges, and opportunities in two-dimensional materials beyond graphene, *ACS Nano*, 2013, **7**, 2898–2926.
- 28 A. Beral, J. Bera and S. Sahu, Low-temperature thermoelectric behavior and impressive optoelectronic properties of two-dimensional XI₂ (X= Sn, Si): A first principle study, *Comput. Mater. Sci.*, 2021, **186**, 109977.
- 29 D. Li, Y. Gong, Y. Chen, J. Lin, Q. Khan, Y. Zhang, Y. Li, H. Zhang and H. Xie, Recent Progress of Two-Dimensional Thermoelectric Materials, *Nano-Micro Lett.*, 2020, **12**, 36.
- 30 K. Hippalgaonkar, Y. Wang, Y. Ye, D. Y. Qiu, H. Zhu, Y. Wang, J. Moore, S. G. Louie and X. Zhang, High thermoelectric power factor in two-dimensional crystals of MoS₂, *Phys. Rev. B*, 2017, **95**, 115407.
- 31 W. Huang, H. Da and G. Liang, Thermoelectric performance of MX₂ (M Mo, W; X S, Se) monolayers, *J. Appl. Phys.*, 2013, **113**, 104304.
- 32 J. Zhang, Y. Xie, Y. Hu and H. Shao, Remarkable intrinsic ZT in the 2D PtX₂ (X= O, S, Se, Te) monolayers at room temperature, *Appl. Surf. Sci.*, 2020, **532**, 147387.
- 33 M. K. Mohanta, A. Rawat, N. Jena, R. Ahammed and A. De Sarkar, Ultra-low lattice thermal conductivity and giant phonon–electric field coupling in hafnium dichalcogenide monolayers, *J. Phys. Condens. Matter*, 2020, **32**, 315301.
- 34 F. Khan, H. U. Din, S. A. Khan, G. Rehman, M. Bilal, C. V. Nguyen, I. Ahmad, L.-Y. Gan and B. Amin, Theoretical investigation of electronic structure and thermoelectric properties of MX₂ (M= Zr, Hf; X= S, Se) van der Waals heterostructures, *J. Phys. Chem. Solids*, 2019, **126**, 304–309.
- 35 G. Li, G. Ding and G. Gao, Thermoelectric properties of SnSe₂ monolayer, *J. Phys. Condens. Matter*, 2016, **29**, 15001.
- 36 J. Li, J. Shen, Z. Ma and K. Wu, Thickness-controlled electronic structure and

- thermoelectric performance of ultrathin SnS₂ nanosheets, *Sci. Rep.*, 2017, **7**, 1–9.
- 37 A. Shafique, A. Samad and Y.-H. Shin, Ultra low lattice thermal conductivity and high carrier mobility of monolayer SnS₂ and SnSe₂: a first principles study, *Phys. Chem. Chem. Phys.*, 2017, **19**, 20677–20683.
- 38 G. Ding, G. Y. Gao, Z. Huang, W. Zhang and K. Yao, Thermoelectric properties of monolayer MSe₂ (M = Zr, Hf): Low lattice thermal conductivity and a promising figure of merit, *Nanotechnology*, 2016, **27**, 1–7.
- 39 J. Bera and S. Sahu, Strain induced valley degeneracy: a route to the enhancement of thermoelectric properties of monolayer WS₂, *RSC Adv.*, 2019, **9**, 25216–25224.
- 40 S.-D. Guo, Biaxial strain tuned thermoelectric properties in monolayer PtSe₂, *J. Mater. Chem. C*, 2016, **4**, 9366–9374.
- 41 G. Li, K. Yao and G. Gao, Strain-induced enhancement of thermoelectric performance of TiS₂ monolayer based on first-principles phonon and electron band structures, *Nanotechnology*, 2017, **29**, 15204.
- 42 Y. Cai, H. Zhou, G. Zhang and Y.-W. Zhang, Modulating Carrier Density and Transport Properties of MoS₂ by Organic Molecular Doping and Defect Engineering, *Chem. Mater.*, 2016, **28**, 8611–8621.
- 43 M. Naseri, M. Abutalib, M. Alkhambashi, J. Gu, J. Jalilian, A. Farouk and J. Batle, Prediction of novel SiX₂ (X= S, Se) monolayer semiconductors by density functional theory, *Phys. E Low-dimensional Syst. Nanostructures*, 2019, **114**, 113581.
- 44 D. Plašienka, R. Martoňák and E. Tosatti, Creating new layered structures at high pressures: SiS₂, *Sci. Rep.*, 2016, **6**, 37694.
- 45 Y. Wang, S.-Q. Jiang, A. F. Goncharov, F. A. Gorelli, X.-J. Chen, D. Plašienka, R. Martoňák, E. Tosatti and M. Santoro, Synthesis and Raman spectroscopy of a layered SiS₂ phase at high pressures, *J. Chem. Phys.*, 2018, **148**, 14503.
- 46 W. Kohn and L. J. Sham, Self-consistent equations including exchange and correlation

- effects, *Phys. Rev.*, 1965, **140**, A1133.
- 47 P. Giannozzi, S. Baroni, N. Bonini, M. Calandra, R. Car, C. Cavazzoni, D. Ceresoli, G. L. Chiarotti, M. Cococcioni and I. Dabo, QUANTUM ESPRESSO: a modular and open-source software project for quantum simulations of materials, *J. Phys. Condens. matter*, 2009, **21**, 395502.
- 48 J. P. Perdew, JP Perdew, K. Burke, and M. Ernzerhof, *Phys. Rev. Lett.* 78, 1396 (1997)., *Phys. Rev. Lett.*, 1997, **78**, 1396.
- 49 J. P. Perdew, K. Burke and M. Ernzerhof, Generalized gradient approximation made simple, *Phys. Rev. Lett.*, 1996, **77**, 3865.
- 50 G. K. H. Madsen and D. J. Singh, BoltzTraP. A code for calculating band-structure dependent quantities, *Comput. Phys. Commun.*, 2006, **175**, 67–71.
- 51 A. Togo, L. Chaput and I. Tanaka, Distributions of phonon lifetimes in Brillouin zones, *Phys. Rev. B*, 2015, **91**, 94306.
- 52 K. S. Novoselov, A. K. Geim, S. V Morozov, D. Jiang, Y. Zhang, S. V Dubonos, I. V Grigorieva and A. A. Firsov, Electric field effect in atomically thin carbon films, *Science* (80-.), 2004, **306**, 666–669.
- 53 N. D. Drummond, V. Zolyomi and V. I. Fal’Ko, Electrically tunable band gap in silicene, *Phys. Rev. B*, 2012, **85**, 75423.
- 54 G. Qin, Q.-B. Yan, Z. Qin, S.-Y. Yue, M. Hu and G. Su, Anisotropic intrinsic lattice thermal conductivity of phosphorene from first principles, *Phys. Chem. Chem. Phys.*, 2015, **17**, 4854–4858.
- 55 Y. Li, Y. Liao and Z. Chen, Be₂C monolayer with quasi-planar hexacoordinate carbons: a global minimum structure, *Angew. Chemie*, 2014, **126**, 7376–7380.
- 56 J. Bardeen and W. Shockley, Deformation potentials and mobilities in non-polar crystals, *Phys. Rev.*, 1950, **80**, 72.
- 57 B. Radisavljevic, A. Radenovic, J. Brivio, V. Giacometti and A. Kis, Single-layer MoS₂

- transistors, *Nat. Nanotechnol.*, 2011, **6**, 147–150.
- 58 S. Das, W. Zhang, M. Demarteau, A. Hoffmann, M. Dubey and A. Roelofs, Tunable transport gap in phosphorene, *Nano Lett.*, 2014, **14**, 5733–5739.
- 59 F. Li, X. Liu, Y. Wang and Y. Li, Germanium monosulfide monolayer: a novel two-dimensional semiconductor with a high carrier mobility, *J. Mater. Chem. C*, 2016, **4**, 2155–2159.
- 60 M. Qiao, Y. Chen, Y. Wang and Y. Li, The germanium telluride monolayer: a two dimensional semiconductor with high carrier mobility for photocatalytic water splitting, *J. Mater. Chem. A*, 2018, **6**, 4119–4125.
- 61 Dimple, N. Jena and A. De Sarkar, Compressive strain induced enhancement in thermoelectric-power-factor in monolayer MoS₂nanosheet, *J. Phys. Condens. Matter*, 2017, **29**, 225501.
- 62 M.-K. Han, Y. Jin, D.-H. Lee and S.-J. Kim, Thermoelectric properties of Bi₂Te₃: CuI and the effect of its doping with Pb atoms, *Materials (Basel)*, 2017, **10**, 1235.
- 63 S. Ju, T. Shiga, L. Feng and J. Shiomi, Revisiting PbTe to identify how thermal conductivity is really limited, *Phys. Rev. B*, 2018, **97**, 184305.
- 64 A. Shafique and Y.-H. Shin, Thermoelectric and phonon transport properties of two-dimensional IV–VI compounds, *Sci. Rep.*, 2017, **7**, 1–10.
- 65 R. Yan, J. R. Simpson, S. Bertolazzi, J. Brivio, M. Watson, X. Wu, A. Kis, T. Luo, A. R. Hight Walker and H. G. Xing, Thermal conductivity of monolayer molybdenum disulfide obtained from temperature-dependent Raman spectroscopy, *ACS Nano*, 2014, **8**, 986–993.
- 66 Z. Jin, Q. Liao, H. Fang, Z. Liu, W. Liu, Z. Ding, T. Luo and N. Yang, A revisit to high thermoelectric performance of single-layer MoS₂, *Sci. Rep.*, 2015, **5**, 18342.
- 67 S. Kumar and U. Schwingenschlögl, Thermoelectric response of bulk and monolayer MoSe₂and WSe₂, *Chem. Mater.*, 2015, **27**, 1278–1284.